



Research articles

The competition between magnetocrystalline and shape anisotropy on the magnetic and magneto-transport properties of crystallographically aligned CuCr_2Se_4 thin films



I. Edelman^{a,*}, M. Esters^b, D.C. Johnson^b, G. Yurkin^{a,c}, A. Tarasov^a, M. Rautsky^a, M. Volochaev^a, S. Lyashchenko^a, R. Ivantsov^a, D. Petrov^a, L.A. Solovyov^d

^a Kirensky Institute of Physics, FRC KSC RAS, Krasnoyarsk 660036, Russia

^b Department of Chemistry, University of Oregon, Eugene, OR 97403, USA

^c Siberian Federal University, Krasnoyarsk, 660041, Russia

^d Institute of Chemistry and Chemical Technology FRC "KSC SB RAS", 660036 Krasnoyarsk, Russia

ARTICLE INFO

Article history:

Received 28 April 2017

Received in revised form 26 June 2017

Accepted 6 July 2017

Available online 11 July 2017

Keywords:

Copper selenide

CuCr_2Se_4 films

Magnetic anisotropy

Transverse Kerr effect

Magnetic resonance

Magneto-resistance

ABSTRACT

Crystallographically aligned nanocrystalline films of the ferromagnetic spinel CuCr_2Se_4 were successfully synthesized and their structure and alignment were confirmed by X-ray diffraction and high-resolution transmission electron microscopy. The average size of the crystallites is about 200–250 nm, and their (1 1 1) crystal planes are parallel to the film plane. A good match of the film's electronic structure to that of bulk CuCr_2Se_4 is confirmed by transverse Kerr effect measurements. Four easy (1 1 1) axes are present in the films. One of these axes is oriented perpendicular and three others are oriented at an angle of 19.5° relative to the film plane. The magnetic properties of the films are determined by a competition between the out-of-plane magnetocrystalline anisotropy and the in-plane shape anisotropy. Magnetic measurements show that the dominating type of anisotropy switches from shape to magnetocrystalline anisotropy near 160 K, which leads to a switch of the effective easy axis from inside the film plane at room temperature to perpendicular to the film plane as the temperature decreases. At last, a moderately large, negative value of the low-temperature magneto-resistance was observed for the first time in CuCr_2Se_4 films.

© 2017 Elsevier B.V. All rights reserved.

1. Introduction

The development of spintronics based on the use of the electron spin degrees of freedom requires an effective search for new materials with high spin polarization [1]. Until recently, oxide compounds such as Cr_2O_3 , Fe_3O_4 , $\text{La}_{0.7}\text{Sr}_{0.3}\text{MnO}_3$, etc. were mainly considered as materials for spintronic devices [2–4]. In recent years, more and more attention has been drawn to complex chalcogenides. It can be expected that the transition from ionic bonds in oxides to more covalent bonds in chalcogenides will result in transport properties similar to the properties of semiconductors or metals. One of the most promising groups of materials for this task are the chalcogenide chromium spinels of the general formula MCr_2X_4 (where M = Cd, Co, Cu, Fe, Hg, Zn, and X = S, Se, Te). Many of them have Curie temperatures above room temperature and possess the ability to include a wide variety of atoms into their

structure, which leads to diverse magnetic, magneto-resistive and electrical properties.

CuCr_2Se_4 stands out from the whole series of chromium chalcogenides: It has the highest Curie temperature ($T_C \sim 430$ K) and metallic conductivity, which makes it a promising candidate for applications in spintronics. CuCr_2Se_4 is characterized by the highest value of the magneto-optical Kerr effect in the near infra-red (1.1° for 0.8 eV and 0.6° for 1.25 eV at 295 K [5]), and is found to undergo light-induced changes in the magnetization [3]. Studies of this compound were carried out mainly on bulk crystals [6–11] or nanocrystalline powders [12–22]. However, most suitable for spintronic applications are samples in the form of thin films that can be integrated into silicon based structures.

Only few articles in the literature are devoted to CuCr_2Se_4 films. The first attempt to synthesize polycrystalline CuCr_2Se_4 films was undertaken in 1990 by Berzhanski et al. [23]. In 2007, Bettinger et al. synthesized CuCr_2Se_4 films by pulsed laser deposition on isostructural MgAl_2O_4 substrates. X-ray diffraction confirmed the structure of CuCr_2Se_4 along with secondary phases of Cr_2Se_3 ,

* Corresponding author.

E-mail addresses: davej@uoregon.edu, ise@iph.krasn.ru (I. Edelman).

CuCrSe₂, and Cr_{2.8}Se₄ [24]. Anderson with co-authors suggested the modulated elemental reactants (MER) method [25,26] to fabricate single-phase films of the ternary chalcogenide compounds. This method was applied successfully to synthesize crystallographically aligned CuCr₂Se₄ thin films consisting of large enough crystallites (several hundred nanometers in lateral dimension) with the (1 1 1) planes oriented parallel to the film plane [27]. The almost homogeneous orientation of the (1 1 1) planes of the crystallites in combination with a large negative magneto-crystalline anisotropy that depends strongly on temperature [12] creates conditions where this anisotropy competes with the easy-plane anisotropy characteristics of thin films, which raises promises new interesting effects in the aligned films.

In this paper, we present the magnetic, magneto-optic, and magneto-transport properties of crystallographically aligned CuCr₂Se₄ thin films synthesized with MER technique [27]. X-ray diffraction and high-resolution electron microscopy study confirmed almost ideal orientation of the crystallite (1 1 1) planes inside the film plane. Magneto-optic transverse Kerr effect spectra appear to be close in shape to the polar Kerr effect spectra of bulk CuCr₂Se₄, suggesting identical electronic structures. Magnetic measurements carried out between 4.2 and 300 K revealed their magnetic properties to be governed by the competition between the magnetocrystalline and shape anisotropy, and that the predominant mechanism of magnetization depends on the temperature with a transition at around 155 K. The microwave and magneto-transport temperature changes correlate with that of the static magnetization. These results show that the CuCr₂Se₄ samples studied herein provide an unusual opportunity to probe the competition between anisotropies of different origin on the magnetic properties of a thin film.

2. Experimental

Films were synthesized using the Modulated Elemental Reactants (MER) method as outlined in [27], using multi-layer precursors with the sequence Se-Cr-Cu-Cr-Se. The precursors were deposited onto (1 0 0)-oriented Si wafers in a custom-built physical vapor deposition chamber with pressures inside the vacuum chamber of less than 5×10^{-7} mbar [28]. Se was evaporated using a resistive heater effusion cell, and Cr and Cu were deposited using electron beam guns. The total film thickness of the precursors was approximately 50 nm, and the thickness of the repeated Se-Cr-Cu-Cr-Se layers was approximately 1.6 nm. Relative thicknesses of the elements were calibrated to yield compositions close to that of the desired CuCr₂Se₄ stoichiometry. Samples were annealed in an evacuated ($p \approx 10^{-5}$ mbar), sealed fused silica tube at 400 °C for 1, 2, and 3 days (samples 1, 2, and 3, respectively). CuSe powder (99.5%, Alfa Aesar) was added to generate a positive Se vapor pressure in order to prevent the evaporation of Se off the film.

The structure of the films was determined using X-ray diffraction (XRD) and electron microscopy techniques. XRD patterns were collected using a PANalytical X'Pert PRO (Cu K α) diffractometer in the angular range $2\theta = 10^\circ - 65^\circ$. The lattice parameters of the samples were refined using the full-profile derivative difference method [29]. Cross-sections of the samples were prepared by focus ion beam (FIB) using a FB2100 (40 kV accelerating voltage) with subsequent Ar⁺ polishing at 0.5 kV. Film cross-section images were obtained with Hitachi HT7700 (W-source) transmission electron microscope (TEM) at 110 kV accelerating voltage. Magnetization hysteresis loops were recorded with a QUANTUM Design MPMS-XL system at temperatures between 4.2 and 300 K with magnetic fields applied parallel and perpendicular to the film plane.

Magneto-transport properties were studied using a homebuilt facility based on a helium cryostat, an electromagnet and a Keith-

ley 2400 Source Meter [30]. Magnetoresistance (MR) was measured between 4.2 and 70 K using a standard four-probe technique. MR was defined as:

$$MR(H) = 100\% \cdot \frac{R(H) - R_{\max}}{R_{\max}} \quad (1)$$

where $R(H)$ is the resistance at an external magnetic field strength H , and R_{\max} is the maximum resistance. In the experiment, electric current flowed inside the film plane, and the magnetic field direction changed from $\theta = 0^\circ$ to $\theta = 180^\circ$ degrees relatively to the normal (\vec{n}) of the film plane.

Ferromagnetic resonance spectra were collected between 120 and 350 K with a Bruker Elexsys E580 spectrometer, operating at the X-band (9.7 GHz) and using 100 kHz as the modulation frequency.

Magneto-optical transverse Kerr effect (TKE) measurements were carried out in the region of 1.25–4.25 eV using an Ellips-891 high speed spectral ellipsometer in an experimental setup described elsewhere [31]. The relative changes of the intensity of the linearly polarized light reflected from the sample surface when changing the direction of the external magnetic field were used as the measured values:

$$\frac{\delta I}{I}(\theta_1, \theta_2) = 2 \frac{I_\uparrow - I_\downarrow}{I_\uparrow + I_\downarrow} \quad (2)$$

where I_\uparrow and I_\downarrow are the intensities of the light incident on the photodetector at the sample during magnetization reversal, $\theta_1 = -45^\circ$ and $\theta_2 = +45^\circ$ are the angles of the polarizer and analyzer rotation relative to the light incidence plane of the sample. The angle of the light incidence with respect to the normal of the film surface was 70° . The magnetic field strength parallel to the film surface changed from +3 to -3 kOe. To minimize the error in the determination of $\delta I/I$, the measurements of I_\uparrow and I_\downarrow were performed 10 times, followed by the calculation of the mean values $\langle I_\uparrow \rangle$ and $\langle I_\downarrow \rangle$, as well as mean-square deviations ΔI_\uparrow and ΔI_\downarrow . The magnetic field dependence of $\delta I/I$ of each sample were obtained for several wavelengths.

3. Results and discussion

3.1. Structure of the CuCr₂Se₄ films

The X-ray diffraction patterns of three CuCr₂Se₄ films annealed for different periods are shown in Fig. 1. The reflections of all samples match completely with CuCr₂Se₄ spinel structure ($Fd\bar{3}m$, No. 225, JCPDS 33-0452). The reflections can be indexed with the (hhh) ($h = 1, 2, 4$) indices of the spinel structure, suggesting a crystallographically aligned structure. Comparing the diffraction patterns shown in Fig. 1 with the XRD patterns presented in Ref. [27] for the CuCr₂Se₄ films synthesized with the same method, one can note some minor differences. Intensities of all reflections for samples 1 and 2 are close to each other, while they are noticeably lower for sample 3. However, no additional reflections are seen for sample 3 compared to samples 1 and 2. The lattice parameters are also close for samples 1 and 2 with 10.310(1) Å and 10.311(1) Å, respectively. For sample 3, the lattice parameter is 10.307(1) Å. The lattice parameters shown for samples 1 and 2 in Ref. [27] were 10.315(3) Å and 10.306(1) Å. The minor differences in the characteristics of the samples synthesized here and presented in Refs. [26,27] fabricated with the same method are well within the experimental errors.

TEM and High-resolution TEM (HRTEM) measurements show that the films consist of well-shaped rectangular nanocrystals with lateral dimensions of a few hundred nanometers and a thickness of 50 nm (Fig. 2a and b). The spaces between two adjacent lattice

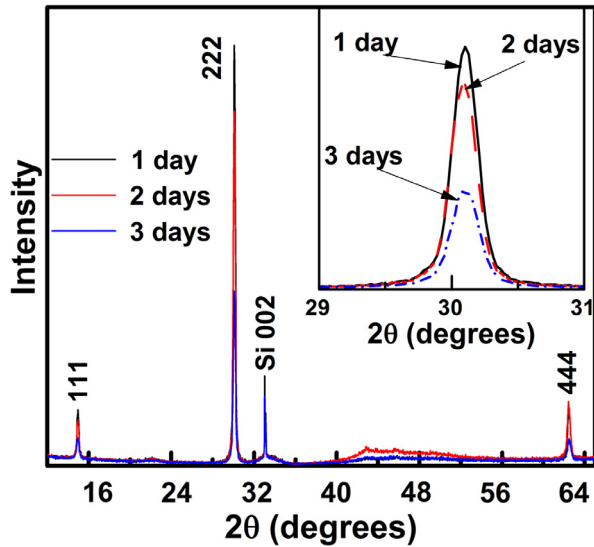


Fig. 1. X-ray diffraction pattern of three CuCr_2Se_4 films annealed for 1, 2, and 3 days. Inset: enlarged region near $2\theta = 30^\circ$.

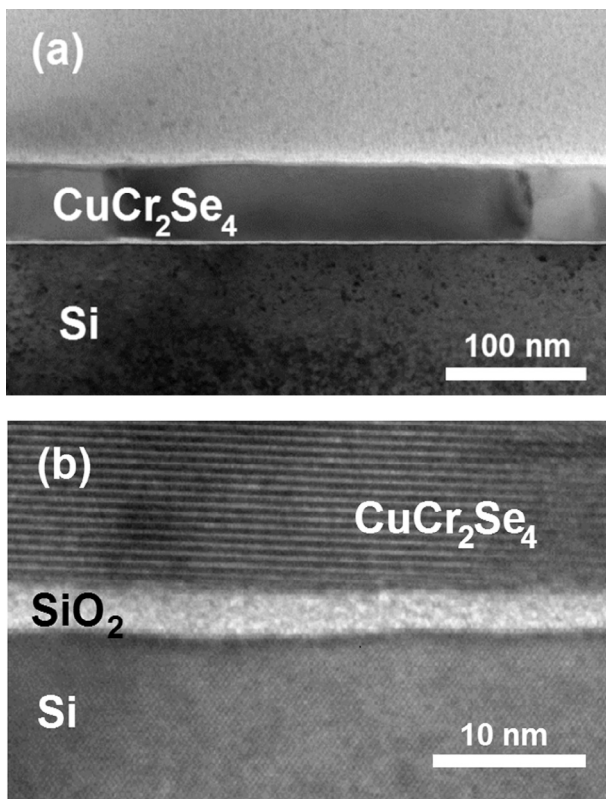


Fig. 2. TEM (a) and HRTEM (b) images of the cross-section of sample 1.

planes in the direction perpendicular to the film surface is 2.68 \AA , which is characteristic for the interplanar (1 1 1) distance in the face-centered cubic phase of CuCr_2Se_4 . The X-ray diffraction and HRTEM data are consistent with the films consisting of pure CuCr_2Se_4 nanocrystals with the (1 1 1) planes oriented parallel to the film surface. Apart from the degree of crystallographic alignment, only insignificant differences are seen between the structural characteristics of films with different annealing times.

3.2. Magnetic hysteresis loops

Fig. 3 represents the magnetization temperature dependence for sample 1 showing the Brillouin-type behavior. For the other two samples, the $M(T)$ curves are analogous. The Curie temperature is $T_C = 420 \text{ K}$, which is a little bit higher compared to those presented in Refs. [24,27] for thin films ($T_C = 405 - 410 \text{ K}$), but lower than the T_C found in bulk ($T_C > 430 \text{ K}$) [12].

The magnetization of the films parallel and perpendicular to the film plane as a function of the external magnetic field H were identical for all samples, and representative data from sample 1 at different temperatures is shown in Fig. 4. We will focus on the data for sample 1 because it has the highest degree of crystallographic alignment compared to the other samples. At room temperature, relatively narrow hysteresis loops close in shape to those presented in Ref. [27] are observed for both orientations of an external magnetic field, parallel and perpendicular to the films surface (curves 1 in Fig. 4a and b). Room temperature coercive fields H_C are of 140 Oe, 135 Oe, and 150 Oe (for samples 1, 2 and 3, respectively). The only noticeable difference between hysteresis loops recorded at the two magnetic field directions is the magnetization behavior in relatively high magnetic fields. While in the parallel geometry, magnetic saturation occurs at $H = 2.0 \text{ kOe}$, for the perpendicular geometry, saturation is not reached at $H = 5 \text{ kOe}$.

A decrease in temperature results in strong changes in the shape of the magnetization curves. For the parallel magnetic field direction, the coercive field decreases slightly and the magnetization does not reach saturation up to $H = 5 \text{ kOe}$ (Fig. 4a), while for the perpendicular magnetic field direction, the coercivity increases approximately an order of magnitude from 140 Oe to 1.6 kOe when the temperature decreases from 300 to 4.2 K (Fig. 4b). The area of the hysteresis loop increases from 7 emu·Oe to 56 emu·Oe for the perpendicular geometry and stays almost unchanged in the parallel geometry. These changes can be explained with the coexistence of two types of magnetic anisotropy in the CuCr_2Se_4 films: the shape anisotropy, which tends to orient the magnetic moment inside the film plane, and the magneto-crystalline anisotropy, which tends to orient the magnetic moment along one of the easy axes. These two types of anisotropy possess different temperature dependences. The field of the in-plane shape anisotropy H_{sh} is described by the equation:

$$H_{sh} = 4\pi M_s \quad (3)$$

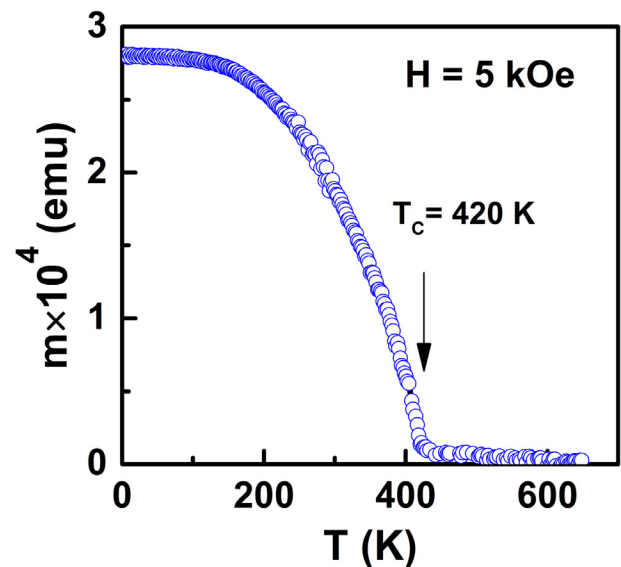


Fig. 3. Temperature-dependent magnetization curve for sample 1.

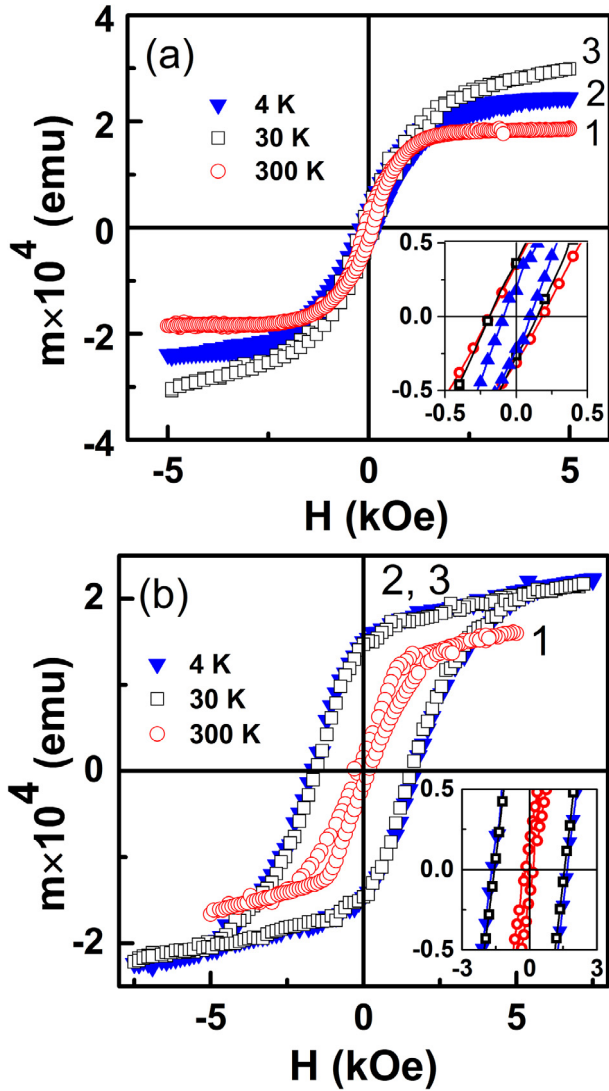


Fig. 4. Magnetization curves of sample 1 recorded for the external magnetic field directions parallel (a) and perpendicular (b) to the film plane at 300, 30, and 4.2 K. Insets: enlarged regions of lower fields.

where M_s is the saturation magnetization, so its temperature dependence is determined by the temperature dependence of M_s . As it is shown in Ref. [27], the magnetization of the film increases strongly near the Curie temperature (420 K) and changes insignificantly with decreasing temperature below 300 K.

The magneto-crystalline anisotropy of CuCr_2Se_4 is characterized by easy magnetization axes oriented parallel to the (111) crystal axes and by a very strong temperature dependence of the anisotropy parameter. K_1 , the first anisotropy constant, increases almost one order of magnitude with the temperature decreasing from 300 to 5 K ($K_1 = -6.9 \times 10^5 \text{ erg/cm}^3$ at 5 K, and $K_1 = -0.9 \times 10^5 \text{ erg/cm}^3$ at 290 K [12]). In cubic crystal lattices, there are four crystal axes of the (111) family, one with an angle of 90° and three oriented at an angle $\alpha = 19.5^\circ$ relative to the (111) crystal plane, i.e. the film's plane. A schematic of these easy axes orientations is presented in Fig. 5a. The crystal anisotropy field is given by:

$$H_K = \frac{2K_1}{M_s}, \quad (4)$$

Both M_s and K_1 are temperature dependent. Fig. 5b illustrates the H_{sh} and H_K temperature dependences calculated for the CuCr_2Se_4

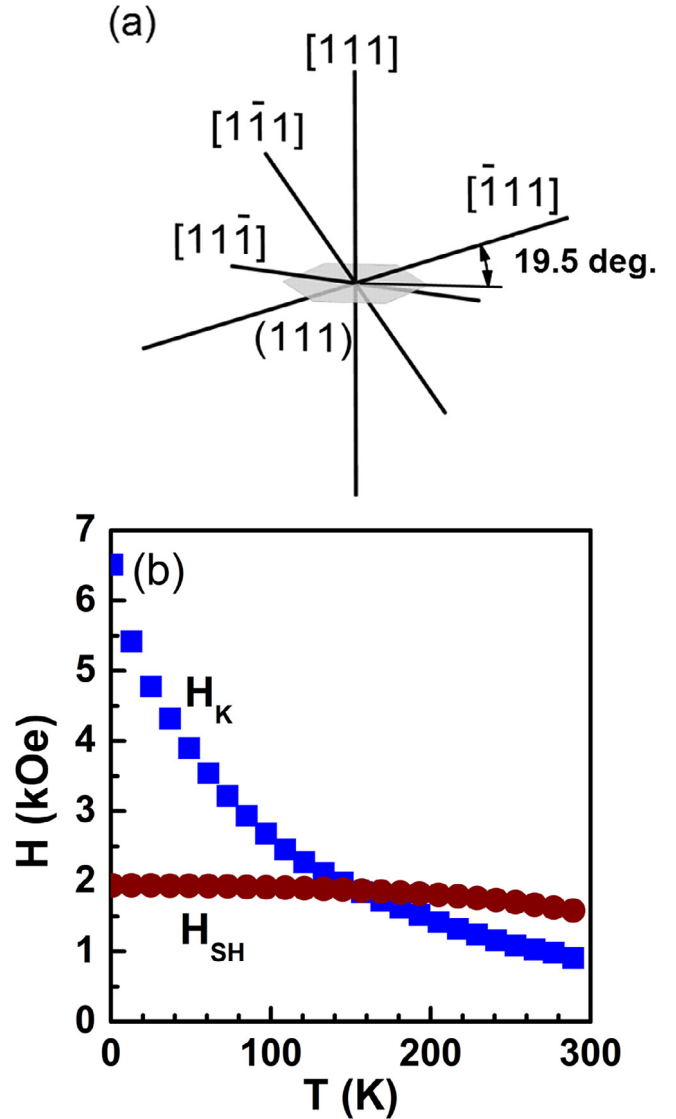


Fig. 5. (a) Schematic of the magneto-crystalline anisotropy easy axes orientation relative to the film plane; (b) Temperature dependence of H_{sh} and H_K calculated according Eqs. (3) and (4) with the M_s temperature dependence taken from Ref. [27] and the K_1 temperature dependence taken from Ref. [12].

thin films using the temperature dependence of M_s taken from Ref. [28] and the temperature dependence of K_1 taken from Ref. [12]. While the temperature dependence of K_1 for these films may be different (magnetocrystalline anisotropy measurements are ongoing), Fig. 5b can provide a good qualitative picture of the temperature dependence of H_{sh} and H_K . The shape anisotropy is nearly temperature independent and H_{sh} increases only slightly when the temperature decreases from 300 K to ~ 160 K, and plateaus at lower temperatures. The magnetocrystalline anisotropy field increases almost one order of magnitude when the temperature decreases from 300 to 4.2 K. At higher temperatures, H_{sh} noticeably exceeds H_K and becomes close to it at approximately 160 K. Below this temperature, H_K starts to prevail and dominates at lower temperatures. This suggests that the magnetic anisotropy can be characterized by an effective anisotropy axis with temperature-dependent orientation.

These findings are consistent with the magnetization measurements. In the parallel geometry of the experiment (magnetic field is parallel to the film plane), the film's magnetic moment remains in the plane or rather close to it, and magnetic saturation occurs at

relatively low field (Fig. 4a). Hysteresis with low coercive force may indicate an involvement of domain wall motion processes along with a rotation of the magnetic moment. Additionally, magnetic moments inside domains are oriented close to the film plane along the effective easy axis located between the external magnetic field direction and one of the magneto-crystalline easy axes $[\bar{1}11]$, $[1\bar{1}1]$, $[11\bar{1}]$ (Fig. 5a). The magnetization process in this case ends with a rotation of the magnetic moment into the film plane. With decreasing temperature, the effective anisotropy axis rotates closer to the magneto-crystalline anisotropy axis, which leads to an increase of the saturated magnetic field.

In the case of the perpendicular geometry, the situation is more complex. The external magnetic field tends to direct the magnetic moment perpendicular to the film plane. However, at higher temperatures, this direction is not energetically favorable. Thus, in low external magnetic fields, magnetic moments locate along one or several of the $[\bar{1}11]$, $[1\bar{1}1]$, $[11\bar{1}]$ axes and the film magnetization process occurs identically to that in the parallel geometry. Further increase of the external magnetic field leads to the rotation of the magnetic moment to the field direction, i.e. to the direction perpendicular to the film plane (Fig. 4b). When the magnetocrystalline anisotropy increases sufficiently at lower temperatures, orienting the magnetic moment along the easy axis normal to the film plane becomes energetically preferable, and after turning off the external field, the magnetic moments tend to keep this orientation. The wide hysteresis loops at 4.2 K and 30 K (Fig. 4b) confirm this explanation. Formation of magnetic domains and the motion of domain walls are also possible mechanisms. Magnetic moments inside domains are oriented perpendicular to the film plane, which reduces the energy of the demagnetizing fields. The relatively large remnant magnetization in this case suggests that in zero external field, a domain structure with domains magnetized predominantly along the previously applied field exists. Thus, the redistribution of the individual contributions of each different type of anisotropy to the magnetization processes can explain the observed magnetization curves. A more detailed study of the magnetization processes is in progress.

3.3. Transverse Kerr effect

Transverse Kerr effect spectra of each sample is presented in Fig. 6. For all three samples, the spectra are very similar to each

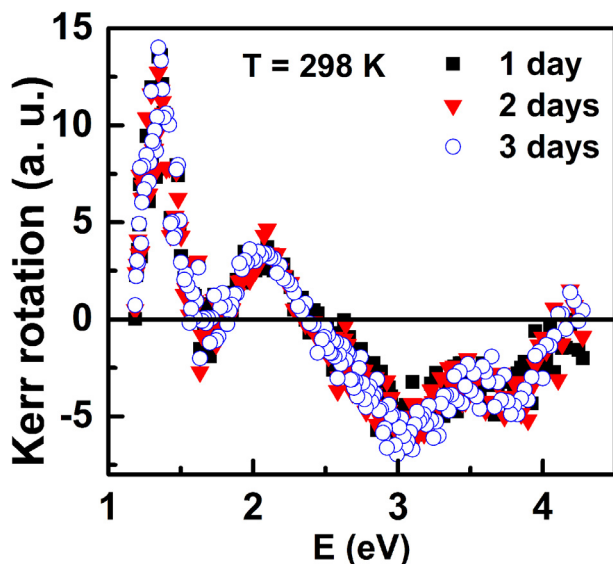


Fig. 6. Room temperature transverse Kerr effect spectra of samples 1, 2, and 3 recorded in magnetic field $H = 3.0$ kOe applied parallel to the films plane.

other, and coincide with the polar Kerr effect spectra observed in several works for CuCr_2Se_4 single crystals [5,8,32] and with the magnetic circular dichroism spectra observed in Ref. [22] for ensembles of CuCr_2Se_4 nanoparticles. As all three effects are due to electronic transitions between energy bands of a substance, it can be concluded that the band structures of the investigated films are identical to the band structure of CuCr_2Se_4 single crystals.

The Kerr effect hysteresis loops are shown in Fig. 7a for sample 1 for the three incident light energies that correspond to the gravity centers of the Kerr spectral maxima ($E = 2.8, 1.4,$ and 1.25 eV). Fig. 7b presents the hysteresis loops of all three samples for $E = 1.25$ eV. These loops correlate well with the magnetic hysteresis loops recorded with the magnetometer at 300 K for the magnetic field directed parallel to the film plane (Fig. 4a), which was expected since the transverse Kerr effect is proportional to the magnetization projection in the film plane.

3.4. Magneto-transport properties

The investigated CuCr_2Se_4 films show negative magnetoresistance (MR) with a maximum of -9% at 4.2 K. The MR dependence

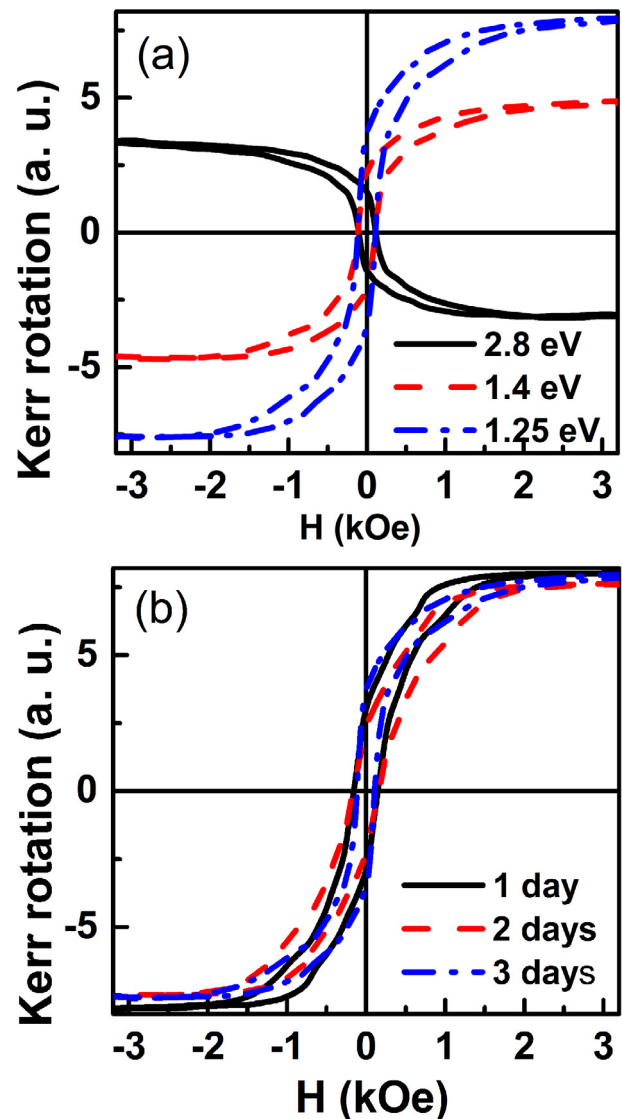


Fig. 7. Room temperature transverse Kerr effect hysteresis loops recorded in magnetic fields parallel to the film plane (a) for sample 1 at three different values of the light wave energy $E = 2.8, 1.4,$ and 1.25 eV, and (b) for all three samples at 1.25 eV.

on the external magnetic field is shown in Fig. 8a for 30 K. The shape of the curves suggests that the MR is mostly due to the film magnetization processes as inferred from the MR hysteresis. There are two mechanisms that are most likely responsible for MR: spin-dependent scattering of charge carriers on domain walls and spin-dependent tunneling between crystallites. The first mechanism is characteristic for all conductive ferromagnetic materials while the latter is characteristic for thin films [33]. Note that the in-plane and out-of-plane MR dependences have the same shape, differing only in width and position of the peaks. In other words, we do not see a difference between the cases where an electric current is applied parallel or perpendicular to the direction of the magnetic field, which indicates that the contribution to the MR associated with the Lorentz force is minimal. Considering that the MR value is only a few percent, one can conclude that spin-dependent tunneling between crystallites is the main mechanism responsible

for the MR effect in the CuCr_2Se_4 thin films. Spin-dependent tunneling between metal (Ni) granules dispersed in SiO_2 films was considered in Ref. [34] where the MR dependence on an external magnetic field was shown to be:

$$MR = -\left(\frac{JP}{4kT}\right) [M^2(H, T) - M^2(0, T)], \quad (5)$$

where P is the polarization of the tunneling electrons, J is the exchange coupling constant within the ferromagnetic metal grains, M is the grain magnetic moment, k is the Boltzmann constant, H is an external magnetic field, T is the temperature. Later, Li et al. [35] have shown that in low magnetic fields, the MR dependence on the external magnetic field can be described in good approximation as:

$$MR \sim \left(\frac{M(H)}{M_s}\right)^2, \quad (6)$$

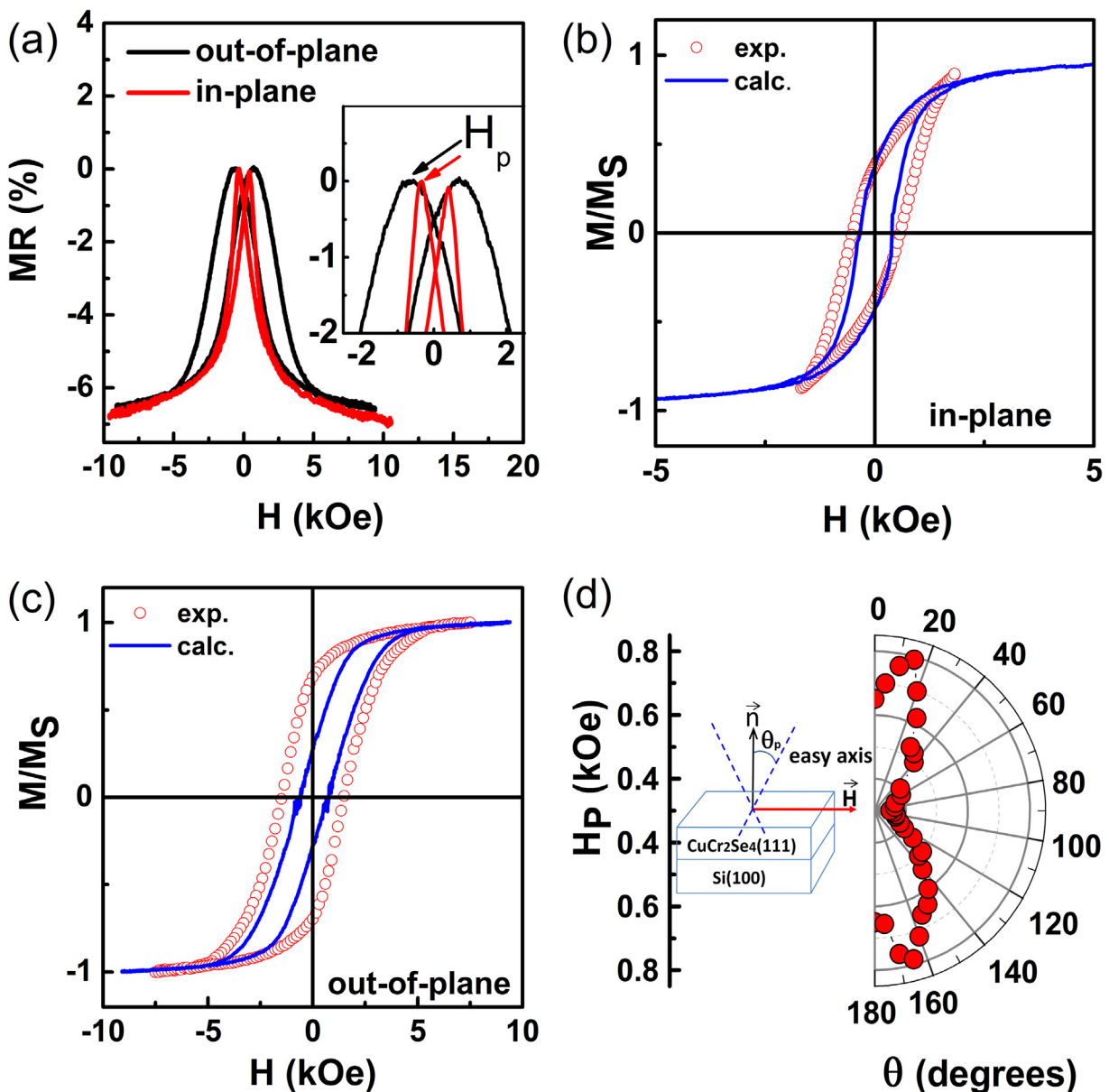


Fig. 8. (a) In-plane and out-of-plane MR as a function of external magnetic field strength H of a CuCr_2Se_4 film at 30 K. Inset: the peak position H_p in the MR dependence on H for the in-plane and out-of-plane geometries. (b, c) Magnetization hysteresis loops calculated from experimental MR(H) with the help of Eq. (6) for the in-plane and out-of-plane geometries, respectively, in comparison with the magnetization experimental hysteresis loops. (d) Polar dependence of the MR hysteresis peak position H_p (right) along with a scheme of the experimental geometry and the directions of the two effective easy axes (left).

where $M(H)$ and M_s are the magnetization in a given field and the saturation magnetization, respectively. We used this approach to calculate the in-plane and out-of-plane magnetization curves from the measured field dependences of the MR. The obtained curves (Fig. 8b and Fig. 8c) correlate well with the experimental magnetization curves (Fig. 4a and b). In particular, the wide hysteresis loop appearing at lower temperatures when the external magnetic field H was applied perpendicular to the film plane was very well reproduced. However, calculated coercive fields for both orientations are lower than experimental ones. This may be due to the fact that in addition to the main MR mechanism, other magnetization mechanisms such as magnetic domain motion and an anisotropic magnetoresistance may contribute to the magnetization. Moreover, in the magnetization processes, the competition of crystal and shape anisotropy played an important role, which makes fitting the hysteresis loops more challenging, especially for the perpendicular magnetic field. Nevertheless, according to the proposed mechanism, the maximum MR should occur near the coercive field because of the randomly oriented magnetic moments of the crystallites in the film plane. Consequently, the peak position H_p in the MR vs. H curves (inset in Fig. 8a) can be interpreted as the coercive field H_c in the magnetization curves. Using MR curves recorded at different angles θ to the film normal, we have obtained the polar dependence of $H_p(\theta)$ that should correspond approximately to $H_c(\theta)$. The results are shown in Fig. 8d. Two distinct maxima at $\theta_p = 15^\circ$ and 165° can

be observed. As the maximal H_c value should be observed when the magnetic field is directed along the easy axis, it is possible that two effective easy axes directed at the angles $\pm 15^\circ$ relative to the film normal occur at 30 K. This is consistent with the temperature dependence of the anisotropy parameters (Fig. 5), which shows that the magnetization is primarily directed along the easy axis [1 1 1], i.e. the normal of the film plane. Note that the effective easy axis orientation at an angle to the film normal can explain the fact that the magnetization does not reach its saturation at low temperatures (Fig. 4b).

3.5. Ferromagnetic resonance

Fig. 9 shows the differential ferromagnetic resonance (FMR) signal recorded at different temperatures of sample 1 with the dc magnetic field H applied parallel (in-plane) and perpendicular (out-of-plane) to the film plane. For the other two films, the results are similar. The resonance signal is a single asymmetric line of Lorentzian shape. Such an asymmetric line shape is generally observed in metallic samples, which confirms the metallic character of the CuCr_2Se_4 films.

The resonance field H_R is defined as the H value where the derivative of P with respect to H is equal to zero:

$$H_R = H \Big|_{\frac{dP}{dH}=0} \quad (7)$$

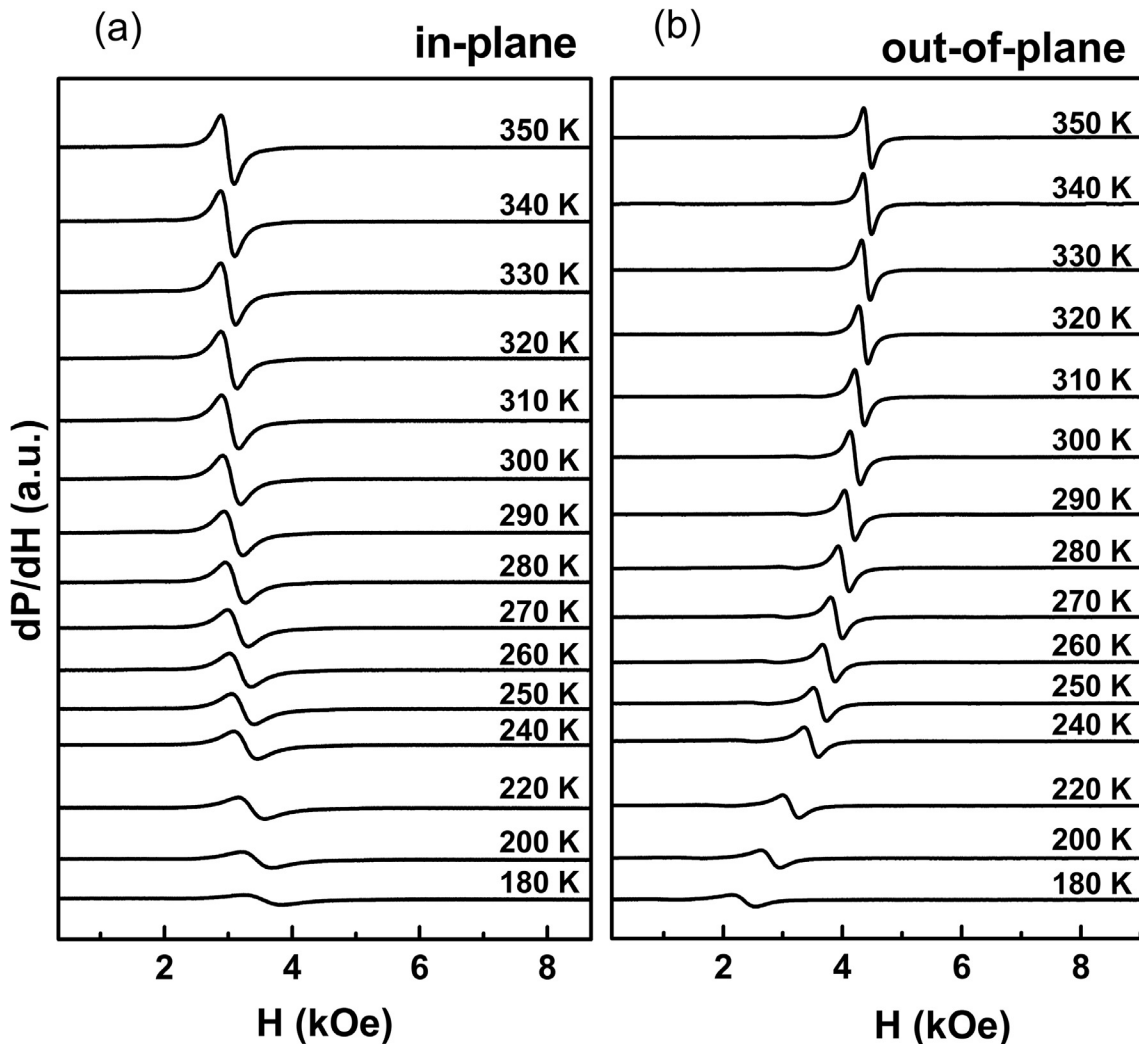


Fig. 9. Differential FMR spectra (dP/dH) at different temperatures for sample 1 with H applied (a) parallel (in-plane) and (b) perpendicular (out-of-plane) to the (1 1 1) plane of the film.

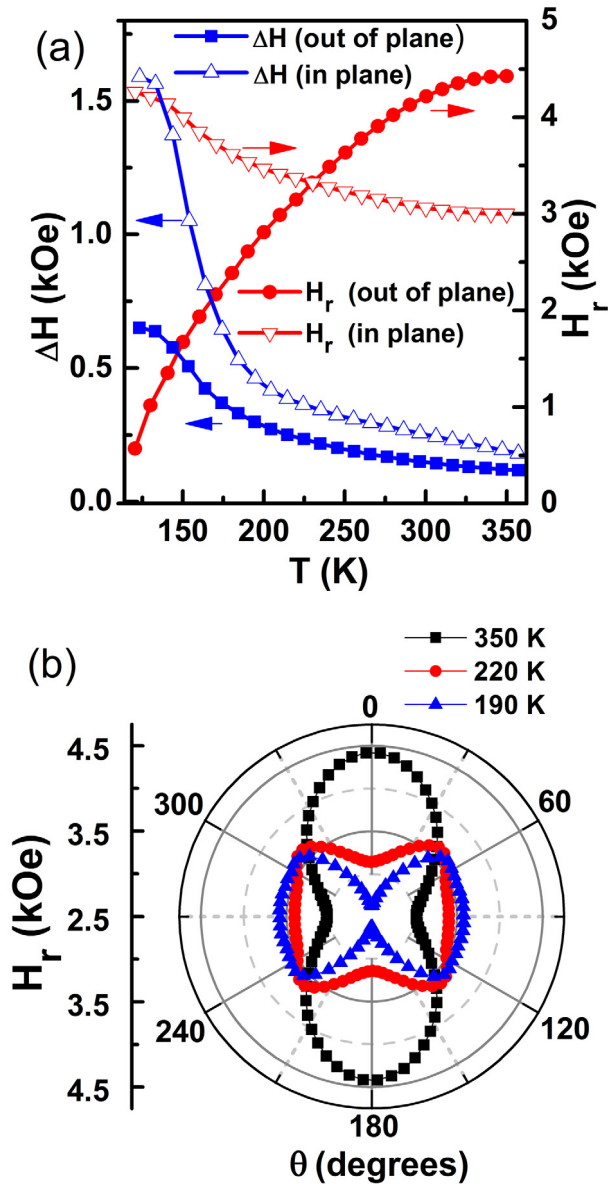


Fig. 10. (a) Temperature dependences of H_R and ΔH_R for sample 1 with H applied perpendicular (filled symbols) and parallel (empty symbols) to the film plane. (b) Polar angle θ dependence of H_R for the same film at different temperatures. $\theta = 0^\circ$ corresponds to the orientation of the $[1\ 1\ 1]$ axis perpendicular to the film plane (see also Fig. 4a).

Here, P is the absorbed microwave power. The temperature dependence of H_R and the resonance line width ΔH_R , which is defined as a distance between positive and negative maxima in the resonance curves, are presented in Fig. 10a. The $H_R(T)$ curves are not typical for films with only in-plane shape anisotropy. For the in-plane and out-of-plane geometries of the experiment, H_R is described by the expressions:

$$\frac{\omega}{\gamma} = H_{R\perp} - 4\pi M_s \quad (8a)$$

$$\left(\frac{\omega}{\gamma}\right)^2 = H_{R\parallel}(H_{R\parallel} + 4\pi M_s) \quad (8b)$$

where ω is the microwave frequency, γ is the gyromagnetic ratio, and $H_{R\perp}$ and $H_{R\parallel}$ are the out-of-plane and the in-plane resonance

fields, respectively. The temperature dependence of H_R is based on the temperature dependence of the saturation magnetization, M_s . As M_s increases with decreasing temperature, $H_{R\perp}$ should increase and $H_{R\parallel}$ should decrease. However, the opposite is observed in the CuCr_2Se_4 as shown in Fig. 9. In order to explain the temperature dependence of H_R observed for our films, we need to take into account the magneto-crystalline anisotropy discussed above, which will lead to the equations:

$$\frac{\omega}{\gamma} = H_{R\perp} - 4\pi M_s - \frac{2K_1}{M_s} \quad (9a)$$

$$\left(\frac{\omega}{\gamma}\right)^2 = H_{R\parallel}\left(H_{R\parallel} + 4\pi M_s + \frac{2K_1}{M_s}\right) \quad (9b)$$

Thus, the temperature dependences of H_R shown in Fig. 10a are determined by the temperature dependence of the magneto-crystalline anisotropy constant, K_1 , to a greater extent than the temperature dependence of the shape anisotropy. To realize this scenario, the magneto-crystalline anisotropy field of a sample should be oriented at an angle to the shape anisotropy field and should increase with decreasing temperature, which is the case for the CuCr_2Se_4 films crystallographically aligned in the $(1\ 1\ 1)$ plane (see Fig. 5). As mentioned earlier, the magneto-crystalline anisotropy is dominated by the shape anisotropy at higher temperatures, and the magneto-crystalline anisotropy starts to prevail at lower temperatures (Fig. 5b), i.e. the direction perpendicular to the film plane is the hard magnetization axis at higher temperatures and becomes the easy magnetization axis at lower temperatures. This is seen very well in the polar angular dependence of H_R (Fig. 10b), where the angle θ is the angle between the direction of an external magnetic field and the normal to the film plane. At $T = 350\text{ K}$, the maximum of H_R corresponds to the hard magnetization axis and is observed when the external magnetic field is normal to the film plane ($\theta = 0^\circ$). The minimum of H_R corresponds to the easy axis and is observed when the external magnetic field is directed within the film plane. This behavior indicates that at room temperature, the magnetic properties of the films are determined by the shape anisotropy. When the temperature decreases to 190 K, the situation is changing dramatically. The minimum of H_R is observed when the external magnetic field is directed normal to the film surface, i.e. this direction becomes the easy direction of magnetization. These results are in good agreement with the results obtained with other techniques.

A predominant axis inside the film plane was not determined, which could be due to the random orientations of the crystallites within the film plane [27]. The random orientation of the crystallites inside the plane and the crystallographic alignment outside the plane are likely responsible for the stronger increase of the in-plane resonance line width with decreasing temperature compared to the out-of-plane line width.

4. Conclusions

Crystallographically aligned nanocrystalline films of ferromagnetic spinel CuCr_2Se_4 were successfully synthesized, and their structure and alignment were confirmed by X-ray diffraction and high-resolution transmission electron microscopy. The average size of the crystallites is of about 200–250 nm, and their $(1\ 1\ 1)$ crystal plane is oriented parallel to the film plane. Transverse Kerr effect spectra coincide with the polar Kerr effect spectra observed for CuCr_2Se_4 single crystals and with the magnetic circular dichroism spectra observed for ensembles of CuCr_2Se_4 nanocrystals, suggesting that the band structure of the investigated films to be the same as in CuCr_2Se_4 crystals.

The combination of the almost ideal crystallite (1 1 1) planes alignment in the film plane, the orientation of the magneto-crystalline easy axes at an angle to this plane, and the in-plane shape anisotropy characteristic for thin films provides a rare opportunity to study the role of the competition between anisotropies of different origin on the magnetic properties of a thin film. The strong temperature dependence of the magneto-crystalline anisotropy along with an almost temperature-independent shape anisotropy below 300 K results in a switch of the easy axis from inside the film plane to perpendicular to the film plane below 160 K, which is responsible for a number of peculiarities of the static and dynamic magnetic properties as well the low temperature magneto-transport properties of the films. In particular, the changes of the hysteresis loop shapes with temperature are remarkably different for magnetic fields applied parallel and perpendicular to the film plane. In the first case, narrow loops with nearly the same coercivity are observed below 300 K, but in the latter case, the coercivity increases with decreasing temperature by almost an order of magnitude. Such a behavior is associated with different mechanisms involved in the films magnetization processes. Data on FMR and magnetoresistance correlate well with the features of the static magnetic properties. A moderately large low-temperature negative magnetoresistance in the CuCr_2Se_4 thin films is observed here for the first time.

Acknowledgements

The work was supported partly by the Grant of the President of the Russian Federation no. NSh-7559.2016.2. M.E. and D.C.J. acknowledge support from the National Science Foundation under grant DMR-1266217.

References

- [1] A. Hirohata, H. Sukegawa, H. Yanagihara, I. Zutic, T. Seki, S. Mizukami, R. Swaminathan, Roadmap for emerging materials for spintronic device applications, *IEEE Trans. Magn.* 51 (2015) 1.
- [2] P. Borisov, A. Hochstrat, V.V. Shvartsman, W. Kleemann, P.M. Hauck, Magnetolectric Cr_2O_3 for spintronic applications, *Integr. Ferroelectr.* 99 (2008) 69.
- [3] Y.X. Lu, J.S. Claydon, E. Ahmad, Y.B. Xua, Hybrid $\text{Fe}_3\text{O}_4/\text{GaAs}(100)/\text{Fe}_3\text{O}_4/\text{GaAs}(100)$ structure for spintronics, *J. Appl. Phys.* 97 (2005) 10C313.
- [4] S. Majumdar, S. van Dijken, Pulsed laser deposition of $\text{La}_{1-x}\text{Sr}_x\text{MnO}_3$: thin-film properties and spintronic applications, *J. Phys. D: Appl. Phys.* 47 (2013), 034010/1–15.
- [5] H. Brandle, J. Schoenes, P. Wachter, Hulliger F and Reim, Large room-temperature magneto-optical Kerr effect in CuCr_2Se_4 , *W. Appl. Phys. Lett.* 56 (1990) 2602.
- [6] D. Kim, K.C. Chung, C.J. Choi, Light induced ferromagnetism of nanocrystalline CuCr_2Se_4 particles, *J. Korean Phys. Soc.* 62 (12) (2013) 2210–2212, <http://dx.doi.org/10.1016/j.jmmm.2007.04.024>.
- [7] V.N. Antonov, V.P. Antropov, B.N. Harmon, A.N. Yaresko, A.Y. Perlov, Fully relativistic spin-polarized LMTO calculations of the magneto-optical Kerr effect of d and f ferromagnetic materials. I. Chromium spinel chalcogenides, *Phys. Rev. B* 59 (1999) 14552.
- [8] S. Bordacs, I. Kezsmarki, K. Ohgushi, Y. Tokura, Experimental band structure of the nearly half-metallic CuCr_2Se_4 : an optical and magneto-optical study, *New J. Phys.* 12 (2010) 053039.
- [9] F. Ogata, T. Hamajima, T. Kambara, K.I. Gondaira, The spin polarized electronic band-structure of chromium spinels.1. CuCr_2S_4 , *J. Phys. C: Sol. St. Phys.* 15 (1982) 3483.
- [10] H. Hahn, C. de Lorent, B. Harder, Untersuchungen über ternäre Chalkogenide. VIII. Über die Struktur des CuV_2S_4 , CuCr_2S_4 , CuCr_2Se_4 und CuCr_2Te_4 , *Z. Anorg. Chem.* 283 (1956) 138.
- [11] F.K. Lotgering, R.P. Van Staple, Magnetic properties and electrical conduction of copper-containing sulfo- and selenospinel, *J. Appl. Phys.* 39 (1968) 417.
- [12] I. Nakatani, H. Nose, K. Masumoto, Magnetic properties of CuCr_2Se_4 single crystals, *J. Phys. Chem. Solids* 39 (1978) 743.
- [13] L. Zhang, W. Tong, J. Fan, C. Zhang, R. Li, Y. Zhang, ESR study of the ferrimagnetic spinel selenide CuCr_2Se_4 , *Eur. Phys. J. B* 83 (2011) 325.
- [14] R. Li, Z. Qu, L. Zhang, L. Ling, W. Tong, Y. Zhang, Structure, magnetic and transport properties of Li-doped CuCr_2Se_4 , *Sol. State Commun.* 150 (2010) 2289.
- [15] S. Bedanta, W. Kleemann, Supermagnetism, *J. Phys. D Appl. Phys.* 42 (2009) 013001.
- [16] K. Ramesha, R. Seshadri, Solvothermal preparation of ferromagnetic sub-micron spinel CuCr_2Se_4 particles, *Sol. St. Sci.* 6 (2004) 841.
- [17] Y. Aktas, O. Akman, M. Ozdem, Preparation of ferromagnetic metallic CuCr_2Se_4 nano-particles by solvothermal chemical reduction reaction methods, *Balkan Phys. Lett.* 15 (2009) 151053.
- [18] C.-R. Lin, C.-L. Yeh, S.-Z. Lu, I.S. Lyubutin, S.-C. Wang, I.P. Suzdalev, Synthesis, characterization and magnetic properties of nearly monodisperse CuCr_2Se_4 nanoparticles, *Nanotechnology* 21 (2010) 235603.
- [19] D. Kim, A.N. Rusnak, S. Parameswaran, C.R. Patra, V.B. Trofimov, R. Harpness, A. Gedanken, Y.S. Tver'yanovich, Preparation and properties of CuCr_2Se_4 ferromagnetic spinel nanocrystals, *Glass. Phys. Chem.* 32 (2006) 330.
- [20] G.M. Tsoi, L.E. Wenger, Y.-H.A. Wang, A. Gupta, Magnetic properties of chalcogenide spinel CuCr_2Se_4 nanocrystals, *J. Magn. Magn. Mater.* 322 (2010) 142.
- [21] M.L. Rao, M. Shamsuzzoha, A. Gupta, Shape-controlled solution synthesis of ferromagnetic copper chromium selenide (CuCr_2Se_4) crystallites, *J. Cryst. Growth* 306 (2007) 321.
- [22] R.D. Ivantsov, I.S. Edelman, S.M. Zharkov, D.A. Velikanov, D.A. Petrov, S.G. Ovchinnikov, C.-R. Lin, O. Li, Y.-T. Tseng, Effects of processing parameters on the morphology, structure, and magnetic properties of $\text{Cu}_{1-x}\text{Fe}_x\text{Cr}_2\text{Se}_4$ nanoparticles synthesized with chemical methods, *J. Alloys Comp.* 650 (2015) 887.
- [23] V.N. Berzhansky, N.A. Drokin, V.I. Ivanov, V.P. Kononov, I.S. Edelman, S.A. Havrichkov, V.K. Chernov, A.G. Shishkov, A.M. Pirogova, Synthesis and physical properties of chalcogenide chromium spinel films, *Thin Solid Films* 190 (1990) 199–215.
- [24] J.S. Bettinger, R.V. Chopdekar, M. Liberatic, J.R. Neulingere, M. Chshiev, Y. Takamura, L.M.B. Alldredge, E. Arenholz, Y.U. Idzerda, A.M. Stacy, W.H. Butlerf, Y. Suzuki, Magnetism and transport of CuCr_2Se_4 thin films, *J. Magn. Magn. Mater.* 318 (2007) 65.
- [25] M.D. Anderson, J. Roberts, K. Kirchgessner, L. LaRossa, I.M. Anderson, D.C. Johnson, Characterization of thin film CuCr_2Se_4 synthesized by a modulated elemental reactant deposition, *Microsc. Microanal.* 15 (Suppl 2) (2009) 550.
- [26] M.D. Anderson, J.O. Thompson, D.C. Johnson, Avoiding binary compounds as reaction intermediates in solid state reactions, *Chem. Mater.* 25 (2013) 3996, <http://dx.doi.org/10.1021/cm4019259>.
- [27] Marco Esters, Andreas Liebig, Jeffrey J. Ditto, Matthias Falmbigl, Manfred Albrecht, David C. Johnson, Synthesis, structure and magnetic properties of crystallographically aligned CuCr_2Se_4 thin films, *J. Alloys Compd.* 671 (2016) 220, <http://dx.doi.org/10.1016/j.jallcom.2016.02.025>.
- [28] L. Fister, X.-M. Li, J. McConnell, T. Novet, D.C. Johnson, Deposition system for the synthesis of modulated, ultrathin-film composites, *J. Vac. Sci. Technol. A* 11 (1993) 3014, <http://dx.doi.org/10.1116/1.578290>.
- [29] H.M. Rietveld, The rietveld method: a retrospection, *Z. Kristallogr.* 225 (2010) 545.
- [30] N.V. Volkov, A.S. Tarasov, E.V. Eremin, F.A. Baron, S.N. Varnakov, S.G. Ovchinnikov, Extremely large magnetoresistance induced by optical irradiation in the $\text{Fe}/\text{SiO}_2/\text{p-Si}$ hybrid structure with Schottky barrier, *J. Appl. Phys.* 114 (2013) 093903.
- [31] S.A. Lyashchenko, I.A. Tarasov, S.N. Varnakov, D.V. Shevtsov, V.A. Shvets, V.N. Zabluda, S.G. Ovchinnikov, N.N. Kosyrev, G.V. Bondarenko, S.V. Rykhliitskii, In situ investigations of magnetooptical properties of thin Fe layers, *Tech. Phys.* 58 (2013) 1529.
- [32] H. Brandle, J. Schoenes, P. Wachter, F. Hulliger, W. Reim, Large room-temperature magneto-optical Kerr effect in $\text{CuCr}_2\text{Se}_{4-x}\text{Br}_x$ ($x = 0$ and 0.3), *J. Magn. Magn. Mater.* 93 (1991) 207.
- [33] A.S. Tarasov, M.V. Rautskii, A.V. Lukyanenko, M.N. Volochaev, E.V. Eremin, V.V. Korobtsov, V.V. Balashev, V.A. Vikulov, L.A. Solovoyov, N.V. Volkov, Magnetic, transport, and magnetotransport properties of the textured Fe_3O_4 thin films reactively deposited onto SiO_2/Si , *J. Alloy. Compd.* 688 (2016) 1095–1100.
- [34] J.S. Helman, B. Abeles, Tunneling of Spin-Polarized Electrons and Magnetoresistance in Granular Ni Films, *Phys. Rev. Lett.* 37 (1976) 1429.
- [35] P. Li, L.T. Zhang, W.B. Mi, E.Y. Jiang, H.L. Bai, Origin of the butterfly-shaped magnetoresistance in reactive sputtered epitaxial films, *J. Appl. Phys.* 106 (2009) 033908, <http://dx.doi.org/10.1063/1.3187537>.